

Detection of Burned Areas through Spectral Indices Analysis of Sentinel-2A Satellite Images in the Abokouamékro Wildlife Reserve (Central, Côte d'Ivoire)

Bob Kouakou Kouadio^{1,2}, Sié Ouattara^{1,2,3}, Alain Clément⁴, Jean-Marc Gala Bi Zaouri², Jean-Luc Kouadio Kouassi Jean-Luc², Edouard Kouakou N'guessan^{5,6}

¹Laboratoire des Sciences et Technologies de la Communication et de l'Information (LSTCI), Institut National Polytechnique Houphouët Boigny (INP-HB), Yamoussoukro, Côte d'Ivoire

²Laboratoire des Sciences Agronomiques et Génie Rural, Institut National Polytechnique Houphouët Boigny (INPHB), Yamoussoukro, Côte d'Ivoire

³Ecole de Géomatique et du Territoire (EGT), Abidjan, Côte d'Ivoire

⁴LARIS, SFR MATHSTIC, Université d'Angers, Angers, France

⁵Centre Universitaire de Recherche et d'application en Télédétection (CURAT), UFR des Sciences de la Terre et des Ressources Minières, Abidjan, Côte d'Ivoire

⁶Laboratoire de Botanique, UFR Biosciences, Université Félix Houphouët Boigny, Abidjan, Côte d'Ivoire
Email: sie_ouat@yahoo.fr

How to cite this paper: Kouadio, B.K., Ouattara, S., Clément, A., Zaouri, J.-M.G.B., Jean-Luc, J.-L.K.K. and N'guessan, E.K. (2024) Detection of Burned Areas through Spectral Indices Analysis of Sentinel-2A Satellite Images in the Abokouamékro Wildlife Reserve (Central, Côte d'Ivoire). *Open Journal of Applied Sciences*, 14, 205-222.
<https://doi.org/10.4236/ojapps.2024.141016>

Received: December 16, 2023

Accepted: January 28, 2024

Published: January 31, 2024

Copyright © 2024 by author(s) and Scientific Research Publishing Inc. This work is licensed under the Creative Commons Attribution International License (CC BY 4.0).
<http://creativecommons.org/licenses/by/4.0/>



Open Access

Abstract

In Côte d'Ivoire, the recurring and unregulated use of bushfires, which cause ecological damage, presents a pressing concern for the custodians of protected areas. This study aims to enhance our comprehension of the dynamics of burnt areas within the Abokouamékro Wildlife Reserve (AWR) by employing the analysis of spectral indices derived from satellite imagery. The research methodology began with the calculation of mean indices and their corresponding spectral sub-indices, including NDVI, SAVI, NDWI, NDMI, BAI, NBR, TCW, TCG, and TCB, utilizing data from the Sentinel-2A satellite image dated January 17, 2022. Subsequently, a fuzzy classification model was applied to these various indices and sub-indices, guided by the degree of membership α , with the goal of effectively distinguishing between burned and unburned areas. Following the classification, the accuracies of the classified indices and sub-indices were validated using the coordinates of 100 data points collected within the AWR through GPS technology. The results revealed that the overall accuracy of all indices and sub-indices declines as the degree of membership α decreases from 1 to 0. Among the mean spectral indices, NDVI-mean, SAVI-mean, NDMI-mean exhibited the highest over-

all accuracies, achieving 97%, 95%, and 90%, respectively. These results closely mirrored those obtained by sub-indices using band 8 (NDVI-B8, SAVI-B8, and NDMI-B8), which yield respective overall accuracies of 93%, 92%, and 89%. At a degree of membership $\alpha = 1$, the estimated burned areas for the most effective indices encompassed 2144.38 hectares for NDVI-mean, 1932.14 hectares for mean SAVI-mean, and 4947.13 hectares for mean NDMI-mean. A prospective approach involving the amalgamation of these three indices could have the potential to yield improved outcomes. This study could be a substantial contribution to the discrimination of bushfires in Côte d'Ivoire.

Keywords

Spectral Indices, Wildfire, Burned Areas, Abokouamékro Wildlife Reserve, Côte d'Ivoire

1. Introduction

Bushfires are recognized as one of the most widespread ecological disturbances globally, alongside natural disasters such as droughts, floods, or hurricanes [1]. Indeed, every year, approximately 350 million hectares of vegetation burn worldwide, with nearly half of this occurring in sub-Saharan Africa [2]. Although the use of bushfires is highly beneficial for humans in land preparation for agriculture, pasture renewal for livestock, and hunting practices, their recurrent and uncontrolled use disrupts forest ecosystems [3]. A recent study conducted by [4] highlighted that 2.7 million hectares burn every year mostly in savannah and forest ecosystems. These fires lead to a decrease in biodiversity and soil fertility loss [5].

In Côte d'Ivoire, village committees for bushfire control have been established by the government. Researchers like [6] and [7] have proposed earlier fires as solution to uncontrolled fires through their experimentations installed respectively in Kokondekro and Lamto. Despite these initiatives, effective solutions to this situation have not been found yet. So each year, bushfires continue to cause damages in different regions. The Abokouamékro Wildlife Reserve (AWR), located in the central region of Côte d'Ivoire, is not immune to this scourge. This protected area, which houses a diverse wealth of flora and fauna, regularly faces forest fires and the spatiotemporal dynamics of which remain poorly understood by managers [8]. Therefore, it is necessary to seek alternative and complementary solutions to existing ones.

Today, the use of satellite remote sensing offers significant opportunities for detecting and monitoring these fires in a given area [3]. Detecting burnt areas using satellite images is a continuously evolving discipline with significant implications for forest fire management. One approach to bushfire management is to have a good understanding of the spatiotemporal dynamics of past fires. At

this level, several authors have worked from a global to a local scale. At the global and continental scale, some authors have used medium spatial resolution images to map bushfire areas. These include [9], who characterized burned areas in the Guinean savannahs of Senegal. The advantage of these images is their frequent repetition, providing information at short time intervals. Also, certain images, such as Modis, provide data on bushfires (active fires, burned areas) that are directly usable. At the local scale, high spatial resolution images (Landsat, Spot, Sentinel, PlanetScope, etc.) are required to better understand details about burned areas. Despite their high spatial resolution, they have the drawback of not having frequent information (low repetition). Several researchers, such as [10], have mapped the spatiotemporal dynamics of burned areas in Togo using Landsat ETM+ images. Joachim and Collins [11] compared three methods for detecting burned areas using Landsat ETM+ imagery in the forest-savanna transition zone in Cameroon. Processing these images requires classification models to extract burned areas because there have no directly usable data (active fires or burned areas). Some classification models are applied to spectral indices to detect burned areas. This is the case with the work of [12], which showed that the combination of Normalized Burn Ratio (NBR) and the Normalized Difference Vegetation Index (NDVI) allow for better characterization of burned areas in a region of China. Wenliang Liu *et al.* [13] also showed that the Burned Area Index (BAI) discriminates better burned areas by comparing several spectral indices from HJ satellite images. The work of David Fornacca *et al.* [14] demonstrated that the NBR and the Normalized Difference Moisture Index (NDMI) discriminate better burned areas.

The study we propose aims to analyze the ability of various spectral indices derived from Sentinel-2A images to detect burnt areas in the AWR. Specifically, the objectives are to: 1) Calculate spectral indices from the Sentinel-2A image; 2) discriminate burnt areas from unburned ones by applying a fuzzy classification model; 3) evaluate the different indices based on classification accuracies (confusion matrix) and estimate burned areas.

2. State of Art

The state of the art in the field of wildfire detection using Sentinel-2A images is built upon a variety of approaches and methodologies. For instance, [12] introduced a sophisticated method for detecting burned areas by leveraging spectral indices derived from Sentinel-2A data. Their work emphasized the significance of the Normalized Burn Ratio (NBR) and the Normalized Difference Vegetation Index (NDVI) in enhancing the accuracy of burned surface detection. Martinez *et al.* [15] focused their efforts on mapping burned areas in Mediterranean ecosystems using Sentinel-2A data. Their research highlighted the positive impact of the high spatial resolution of these images for improved forest fire identification in this specific region.

Khan *et al.* [16] explored the application of deep learning algorithms, specifi-

cally Convolutional Neural Networks (CNNs), for detecting burned areas from Sentinel-2A data, providing an in-depth insight into the use of machine learning for this task. The integration of multispectral and thermal infrared data from Sentinel-2A was addressed by [17]. Their study emphasized the utility of thermal infrared in improving forest fire detection and discussed the advantages of this approach.

Davis and Walker [18] developed a methodology for change detection based on time series of Sentinel-2A images, enabling the monitoring of burned areas' evolution over time. In the context of disaster management, Davis and Wilson [19] explored the use of machine learning for rapid assessment of burned areas using Sentinel-2A data, highlighting the importance of speed and accuracy in such emergency situations.

Gonzalez and Rodriguez [20] assessed the usefulness of Sentinel-2A data for mapping burned areas in arid regions, providing crucial insights into the specific challenges of wildfire detection in these environments. Walker and Lopez [21] conducted a comparative analysis of burned area detection methods using Sentinel-2A images in different environments, thus demonstrating the importance of method adaptability depending on the context.

Smith and Miller [22] proposed an ensemble approach for mapping burned areas from Sentinel-2A data, thereby emphasizing the improvement in result reliability through the combination of various methods. Geospatial analysis of burned area severity was explored by [23], enabling the evaluation of fire-induced damages and their impact on the environment using Sentinel-2A data.

Garcia and Brown [24] conducted a comparative study of spectral indices for burned area detection from Sentinel-2A images, offering a detailed overview of the performance of various indices and their respective advantages. In the context of natural reserves, [20] examined the use of Sentinel-2A data for monitoring burned areas, highlighting the importance of remote sensing for biodiversity management in these sensitive environments.

Lastly, [25] evaluated the accuracy of mapping burned areas in urban areas using Sentinel-2A data, shedding light on the specific challenges associated with fire detection in urban settings.

3. Materials and Methods

3.1. Study Area

This study was conducted in the developed part of the AWR located in the heart of the "V Baoulé" region in central Côte d'Ivoire. The AWR was established in 1988 and covers an area of 20,400 hectares, of which 7230 hectares have been developed. The reserve is located between the coordinates of 4°57' and 5°09' West longitude and 6°48' and 6°55' North latitude. Administratively, it belongs to both the Bélier region and the N'Zi region, as well as the autonomous district of Yamoussoukro. It falls within the subequatorial Baoulé climate, characterized by four seasons, including two rainy seasons and two dry seasons. The average

annual precipitation is around 1050 mm, with an average annual temperature of 26°C and an average annual relative humidity of 75%.

The reserve is drained by two main rivers, the Kan and the Pra, along with their various tributaries. The area features ferralitic and remodeled tropical ferruginous soils [26]; the vegetation in the AWR comprises forest formations (gallery forests, forested patches) and savanna formations (wooded savannas, tree savannas, shrub savannas). Forest formations are dominated by species such as *Antiaris toxicaria* (Moraceae), *Aubrevillea kerstingii* (Mimosaceae), *Ceiba pentandra* (Bombacacée), *Cola cordifolia* (Sterculiaceae), *Kaya grandifoliola* (Maliaceae), *Carapa procera* (Meliaceae), and *Elaeis guineensis* (Arecaceae), among others. Savanna formations are characterized by species such as *Borassus aethiopicum* (Arecaceae), *Daniellia oliveri* (Caesalpiniaceae), *Ficus platyphylla* (Moraceae), *Lophira lanceolata* (Ochnaceae), *Parkia biglobosa* (Mimosaceae), *Annona senegalensis* (Annonaceae), *Crossopteryx febrifuga* (Rubiaceae), *Dichrostachyus cinerea* (Mimosaceae), *Hymenocardia acida* (Euphorbiaceae), *Piliostigma thonningii* (Caesalpiniaceae), *Elymandra androphila* (Poaceae), *Hyparrhenia smithiana* (Poaceae), *Imperata cylindrica* (Poaceae), and *Loudetia arundinacea* (Poaceae) [5]. The riparian areas of the AWR are inhabited by both indigenous and non-indigenous populations. The local economy of these communities primarily relies on agriculture, livestock, tourism, and craftsmanship. **Figure 1** depicts the location of the developed zone within the Abokouamékro Wildlife Reserve.

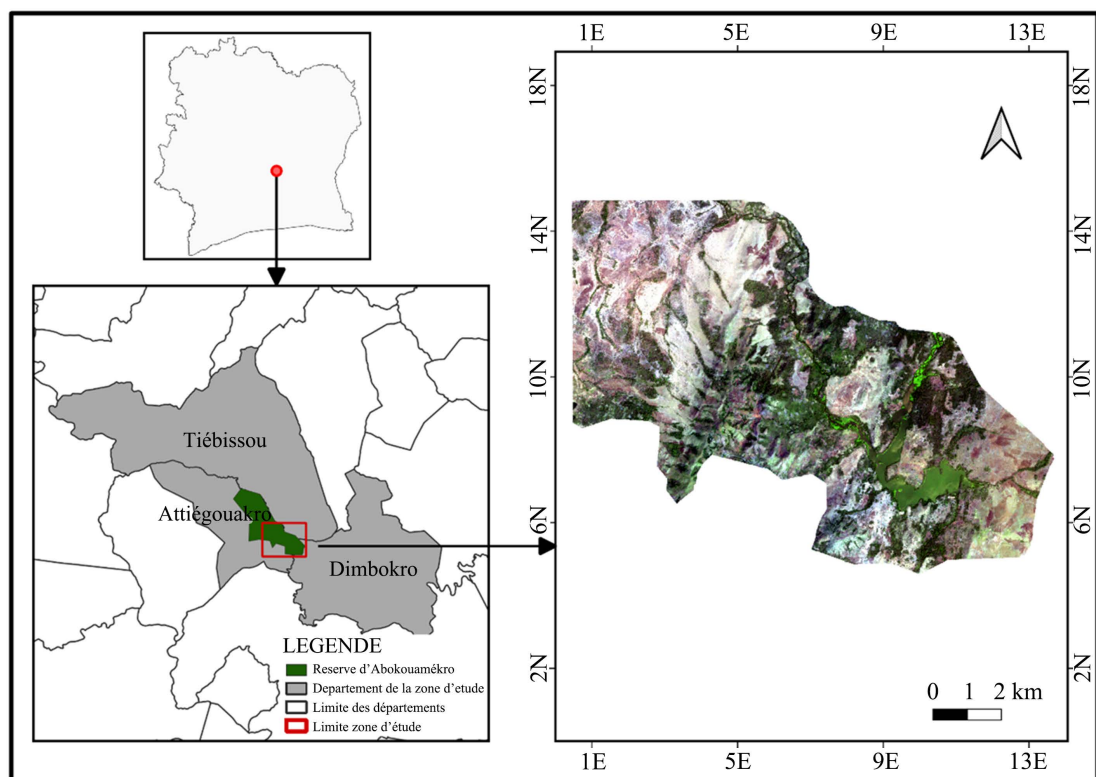


Figure 1. Location of the developed zone within the AWR.

3.2. Data

Two types of data were used in this study. The first type of data includes an image derived from multi-spectral sensors of the Sentinel-2A satellite, which is part of the Sentinel-2 twin satellite system. The Sentinel-2A image used in this article is from January 17, 2022, and is characterized by a 280 km-wide field of view with a revisit period of five days. These images encompass thirteen spectral bands covering the visible and infrared ranges. The visible bands include b1 (band 1), b2 (band 2), b3 (band 3), b4 (band 4), while the near-infrared bands include b5 (band 5), b6 (band 6), b7 (band 7), b8 (band 8), b8A (band 8A), b9 (band 9), b10 (band 10), and the mid-infrared spans b11 (band 11) and b12 (band 12). These spectral bands were used to compute various spectral indices and sub-indices. The characteristics of the Sentinel-2A image are summarized in **Table 1**.

The second type of data consists of Global Positioning System (GPS) coordinates for burned areas collected after bushfires. Data collection took place during field missions from January 25 to January 31, 2022, within the AWR. A total of 250 fixed points, covering burned and unburned areas (vegetation, bare ground, water bodies), were collected to encompass the developed zone of the AWR. Among these 250 points, 150 were used to classify the indices, and the remaining 100 points served to validate the classified indices.

Table 1. Sentinel-2A image characteristics.

	Spectral domain	Band	Wave length (nm)	Spatial resolution (m)
Visible	Coastal Aerosol	b1	442.3 - 443.9	60
	Blue	b2	492.1 - 496.6	10
	Green	b3	559 - 560	10
	Red	b4	664.5 - 665	10
Near Infrared	Red edge1	b5	703.8 - 703.9	20
	Red edge2	b6	739.1 - 740.2	20
	Red edge3	b7	779.7 - 782.5	20
	Near Infrared	b8	833 - 835.1	10
	Near Infrared Narrow	b8A	864 - 864.1	20
	Water Vapor	b9	943.2 - 945	60
	SWIR Citrus	b10	1276.9 - 1373.5	60
Medium Infrared	Short Wave Infrared	b11	1610.4 - 1613.7	20
	Long Wave Infrared	b12	2185.7 - 2202.4	20

3.3. Methods

The methodological approach in this article consists of three phases. The first phase involved preprocessing the image and calculating spectral indices. The second phase focused on classifying the different spectral indices and estimating burned areas. The third phase dealt with the validation of the classified indices.

3.3.1. Image Preprocessing and Spectral Indices Calculation

Image preprocessing and spectral indices calculation were carried out in three phases using ENVI 5.10 software. In the first phase, the raw image was georeferenced to make it compatible with other data sources already possessing geographic coordinates. This process involved generating the coordinates of specific points within the image based on fixed points called “reference points.” Each band from the visible to the infrared was georeferenced using the *k* nearest neighbors’ method.

The second phase involved resizing the pixel dimensions of certain image bands. Specifically, the 20 m dimensions of the b5, b6, b7, b11, and b12 spectral bands and the 60 m dimensions of the b1, b9, and b10 bands were all adjusted to a 10 m size using bilinear interpolation. The study area’s definition was based on a vector file representing the boundaries of the developed part of the reserve. This area corresponds to an extracted image window covering an area of pixels with dimensions 764×754 pixels.

The spectral indices and image transformations considered in this article were selected from a wide range of indices described in the literature. These include seven spectral indices: NDVI (Normalized Difference Vegetation Index), SAVI (Soil-Adjusted Vegetation Index), MNDWI (Modified Normalized Difference Water Index), NDWI (Normalized Difference Water Index), NDMI (Normalized Difference Moisture Index), NBR (Normalized Burned Ratio), BAI (Burned Area Index), MIRBI (Mid-infrared Burned Index), and three image transformations: TCW (Tasseled Cap Wetness), TCG (Tasseled Cap Greenness), and TCB (Tasseled Cap Brightness). The calculation of these parameters involved generating new channels in the spectrum ranging from visible to infrared using the raw image bands. The calculation models and bibliographical references for these spectral indices are presented in **Table 2**.

Among the seven spectral bands b6, b7, b8, b8A, b9, b10 available in the Sentinel-2A image in the near-infrared domain, five have been considered in this article. These are bands b5, b6, b7, b8, and b8A. Five sub-indices corresponding to each of the spectral indices NDVI, SAVI, BAI were calculated by taking the ratio of each of the above-mentioned bands to band b4. Five other sub-indices corresponding to the spectral indices NDMI and NBR were calculated by taking the ratio of each of the near-infrared bands to band b11 for NDMI and band b12 for NBR. Regarding NDWI, five sub-indices were obtained from the ratio of band b3 to each of the near-infrared bands. Furthermore, no sub-spectral indices were calculated for MNDWI, MIRBI, TCW, TCG, TCB. The list of calculated sub-spectral Indexes is presented in **Table 3**.

Table 2. Calculation models and bibliographical references for the spectral indices used.

Indices spectraux	Formule	Référence
Normalized Difference Végétation Index (NDVI)	$\frac{NIR - R}{NIR + R}$	Rousse <i>et al.</i> (1973)
Soil-adjusted Vegetation Index (SAVI)	$\frac{NIR - R}{(NIR + R + 0.5) * 1.5}$	Chuvieco <i>et al.</i> (2002)
Normalized Difference Moisture Index (NDMI)	$\frac{NIR - SWIR}{NIR + SWIR}$	Key and Benson (2000)
Normalized Burned Ratio (NBR)	$\frac{NIR - LWIR}{NIR + LWIR}$	Key and Benson (2000)
Mid-infrared Burned Index (MIRBI)	$10 * LWIR - 9.5 * SWIR + 2$	Trigg and Flasse (2001)
Burned Area Index (BAI)	$\frac{1}{(0.1 + R)^2 + (0.06 + NIR)^2}$	Chuvieco <i>et al.</i> (2002)
Normalized Difference Water Index (NDWI)	$\frac{G - NIR}{G + NIR}$	McFeeters (1996)
Modified Normalized Difference Water Index (MNDWI)	$\frac{G - SWIR}{G + SWIR}$	Xu (2006)
Tasseled Cap Wetness (TCW)	$0.1363 * B + 0.2802 * G + 0.3072 * R + 0.5288 * Re1 + 0.1379 * Re2 - 0.0001 * Re3 - 0.0807 * NIR1 - 0.4064 * SWIR1 - 0.5602 * SWIR2 - 0.1389 * NIR2$	
Tasseled Cap Greeness (TCG)	$0.1363 * B + 0.2802 * G + 0.3072 * R + 0.5288 * Re1 + 0.1379 * Re2 - 0.0001 * Re3 - 0.0807 * NIR1 - 0.4064 * SWIR1 - 0.5602 * SWIR2 - 0.1389 * NIR2$	
Tasseled Cap Brighthness (TCB)	$0.1363 * B + 0.2802 * G + 0.3072 * R + 0.5288 * Re1 + 0.1379 * Re2 - 0.0001 * Re3 - 0.0807 * NIR1 - 0.4064 * SWIR1 - 0.5602 * SWIR2 - 0.1389 * NIR2$	

Table 3. List of calculated sub-spectral indexes.

Index	Sub-Spectral Indexes
NDVI	NDVI-b5, NDVI-b6, NDVI-b7, NDVI-b8, NDVI-b8A
SAVI	SAVI-b5, SAVI-b6, SAVI-b7, SAVI-b8, SAVI-b8A
BAI	BAI-b5, BAI-b6, BAI-b7, BAI-b8, BAI-b8A
NDWI	NDWI-b5, NDWI-b6, NDWI-b7, NDWI-b8, NDWI-b8A
NDMI	NDMI-b5, NDMI-b6, NDMI-b7, NDMI-b8, NDMI-b8A
NBR	NBR-b5, NBR-b6, NBR-b7, NBR-b8, NBR-b8A

3.3.2. Fuzzy Classification for Burned and Unburned Area Detection

1) Method for Determining Models for Burned and Unburned Areas

Separation thresholds between burned areas and unburned areas (vegetation, bare ground, water bodies) were determined for each spectral index and sub-spectral index. The method involved extracting the pixel values for each spectral index or sub-spectral index from the 150 points collected in the field.

Using this data, statistics such as the mean (μ), standard deviation (σ), minimum value (Min), and maximum value (Max) were calculated for each index and sub-index. The lower and upper bounds for extracting burned pixels were determined using Equation (1).

$$\mu - \sigma \leq x \leq \mu + \sigma \quad (1)$$

where:

x : set of spectral values (index or sub-index) from the 150 points collected in the field,

μ : mean of the spectral values from the 150 points,

σ : standard deviation of the spectral values from the 150 points.

A pixel is considered “burned” when its value falls within the interval defined by the lower and upper bounds calculated above. On the other hand, any pixel with a value outside this interval is considered “unburned.”

2) Determination of Breakpoints in Classification Models

In this study, it is assumed that a pixel belongs to the “burned” class with certainty when it falls within the intervals defined by the lower and upper bounds of all sub-spectral indices. However, any pixel that falls within 2, 3, or 4 out of 5 sub-indices can be considered to belong to the “burned” class with a lower degree of certainty. Pixels located outside all the intervals of all sub-indices are classified as “unclassified.”

To extract these 3 categories of pixels, all sub-indices for each spectral index were intersected to determine their intersections. This operation allowed the construction of fuzzy classification models (Figure 2(a) and Figure 2(b)) for each spectral index. The breakpoints of these models were determined as follows. In Figure 2(a) and Figure 2(b), “a” corresponds to the minimum of the minima lower bounds of all sub-indices. “b” corresponds to the maximum of the minima lower bounds of all sub-indices. “c” corresponds to the minimum of the maxima upper bounds of all sub-indices. “d” corresponds to the maximum of the maxima upper bounds of all sub-indices.

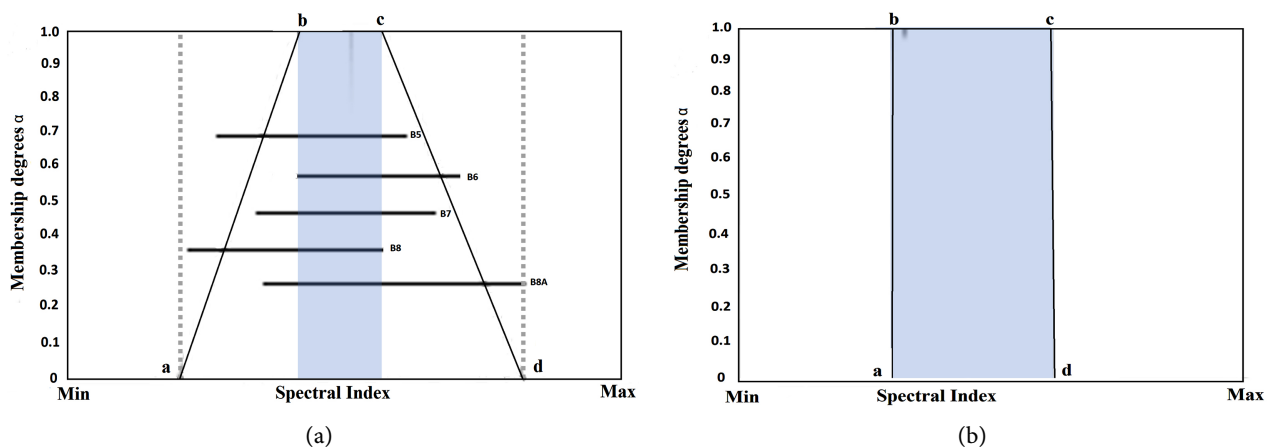


Figure 2. (a): Fuzzy Model for the Classification of NDVI, SAVI, BAI, NDMI, NBR, and NDWI Indices; (b): Fuzzy Model for the Classification of TCW, TCG, TCB, MIRBI, MNDWI indices.

These various models allow assigning a pixel to either the “burned” class or the “unburned” class for different degrees of membership (α), which ranges from 0 to 1. For a high degree of membership ($\alpha \rightarrow 1$), the index values are likely to accurately identify burned pixels. However, as it gradually decreases ($\alpha \rightarrow 0$), we enter the maximum overlap zone between burned and unburned pixels. The degree of membership (α) remains constant ($\alpha = 0$) for all indices without sub-indices (MNDWI, MIRBI, TCW, TCG, TCB); therefore, $a = b$ and $c = d$. The breakpoint values of these models are recorded in **Table 4**.

3) Fuzzy Model for Burned and Unburned Area Classification

The fuzzy model algorithms used in this article were determined as follows. The question at hand is: for a given degree of membership (α), what is the set of pixels X of the index that designate burned pixels? In other words, what are the lower and upper bounds of each index that defines the pixels for a given degree of membership (α)? The different classification algorithms were determined based on the degree α (**Table 5**).

The different algorithm and programming code of these models enabled the generation of spectral indices and sub-indices classified based on the fuzzy membership degree α using Matlab software

4) Evaluation and Validation of Classified Indexes

To assess the discrimination potential of the ten spectral indices, a method based on constructing a confusion matrix (**Table 6**) was employed. The classification confusion matrix was calculated by comparing the results of the classification of burned and unburned areas (predicted data) with the ground truth data (actual data).

From the confusion matrix, indicators for the spectral indices, such as omission, commission, and overall accuracy, were calculated using Equations (2)-(4).

Table 4. Breakpoint values of fuzzy models.

Indices	a	b	c	d
NDVI	0.096	0.146	0.214	0.267
SAVI	0.158	0.235	0.319	0.4
NBR	-0.117	-0.0062	-0.08	-0.031
NDWI	-0.216	-0.157	-0.118	-0.071
NDMI	-0.103	-0.059	0.111	0.171
BAI	$-63 * 10^{-5}$	$59 * 10^{-5}$	$55 * 10^{-5}$	$51 * 10^{-5}$
MNDWI	-0.267	0.207	-0.163	-0.009
MIRBI	0.040	0.040	0.128	0.128
TCW	-342.37	-342.37	-106.36	-106.36
TCG	333.46	333.46	635.06	635.06
TCB	2643.16	2643.16	3244.16	3244.16

Table 5. List of algorithms used for fuzzy models based on degree of membership (α).

Index	If $\alpha = 0$	If $0 < \alpha < 1$	If $\alpha = 1$
NDVI	$0.096 \leq \text{NDVI} \leq 0.267$	$0.096 + 0.050 * \alpha \leq \text{NDVI} \leq 0.267 - 0.053 * \alpha$	$1.46 \leq \text{NDVI} \leq 0.214$
SAVI	$0.158 \leq \text{SAVI} \leq 0.40$	$0.158 + 0.077 * \alpha \leq \text{SAVI} \leq 0.4 - 0.081 * \alpha$	$0.235 \leq \text{SAVI} \leq 0.4$
NDMI	$0.103 \leq \text{NDMI} \leq 0.171$	$0.044 * \alpha - 0.103 \leq \text{NDMI} \leq 0.17 - 0.06 * \alpha$	$-0.059 \leq \text{NDMI} \leq 0.111$
NBR	$-0.117 \leq \text{NBR} \leq -0.031$	$0.055 * \alpha - 0.062 \leq \text{NBR} \leq -0.015 * \alpha - 0.031$	$-0.062 \leq \text{NBR} \leq -0.046$
NDWI	$-0.216 \leq \text{NDWI} \leq -0.071$	$0.059 * \alpha - 0.216 \leq \text{NDWI} \leq -0.047 * \alpha - 0.071$	$-0.157 \leq \text{NDWI} \leq -0.118$
BAI	$-0.00063 \leq \text{BAI} \leq -0.000516$	$0.36 * 10^5 * \alpha - 0.63 * 10^3 \leq \text{BAI} \leq -0.35 * 10^5 * \alpha - 0.51 * 10^3$	$-0.000595 \leq \text{BAI} \leq -0.00051$
MNDWI	$-0.207 \leq \text{MNDWI} \leq -0.163$	$-0.207 \leq \text{MNDWI} \leq -0.163$	$-0.207 \leq \text{MNDWI} \leq -0.163$
MIRBI	$0.040 \leq \text{MIRBI} \leq 0.128$	$0.040 \leq \text{MIRBI} \leq 0.128$	$0.040 \leq \text{MIRBI} \leq 0.128$
TCW	$-342.372 \leq \text{TCW} \leq -106.364$	$-342.372 \leq \text{TCW} \leq -106.364$	$-342.372 \leq \text{TCW} \leq -106.364$
TCG	$333.463 \leq \text{TCG} \leq 635.064$	$333.463 \leq \text{TCG} \leq 635.064$	$333.463 \leq \text{TCG} \leq 635.064$
TCB	$2643.159 \leq \text{TCB} \leq 3244.163$	$2643.159 \leq \text{TCB} \leq 3244.163$	$2643.159 \leq \text{TCB} \leq 3244.163$

Table 6. Classification confusion matrix.

	Predicted Burned Areas	Predicted Unburned Areas
Actual Burned Areas	True Positives (TP)	False Positives (FP)
Actual Unburned Areas	False Negatives (FN)	True Negatives (TN)

$$\text{Omission error} = \frac{\text{FP}}{\text{FP} + \text{FN}} \tag{2}$$

$$\text{Commission error} = \frac{\text{FN}}{\text{VN} + \text{FN}} \tag{3}$$

$$\text{Overall Accuracy} = \frac{\text{VP} + \text{VN}}{\text{VP} + \text{VN} + \text{FP} + \text{FN}} \tag{4}$$

where:

TP: True Positives; FP: False Positives; TN: True Negatives; FN: False Negatives.

The omission error indicates the rate of truly burned pixels that are classified as unburned, which corresponds to the false positive rate (FP). The commission error is the rate of pixels predicted as unburned by the model but classified as burned, which corresponds to the false negative rate (FN). Overall accuracy, or global error rate, represents the general quality of the model. The confusion matrix helps determine and compare index performances in terms of overall accuracy or errors (commission, omission).

The summary of the methodology is illustrated in **Figure 3**.

4. Results and Discussion

4.1. Spectral Indices and Sub-Indices

The spectral indices and sub-indices generated from the raw Sentinel-2A image dated January 17, 2022, are represented by the images listed in **Figure 4**.

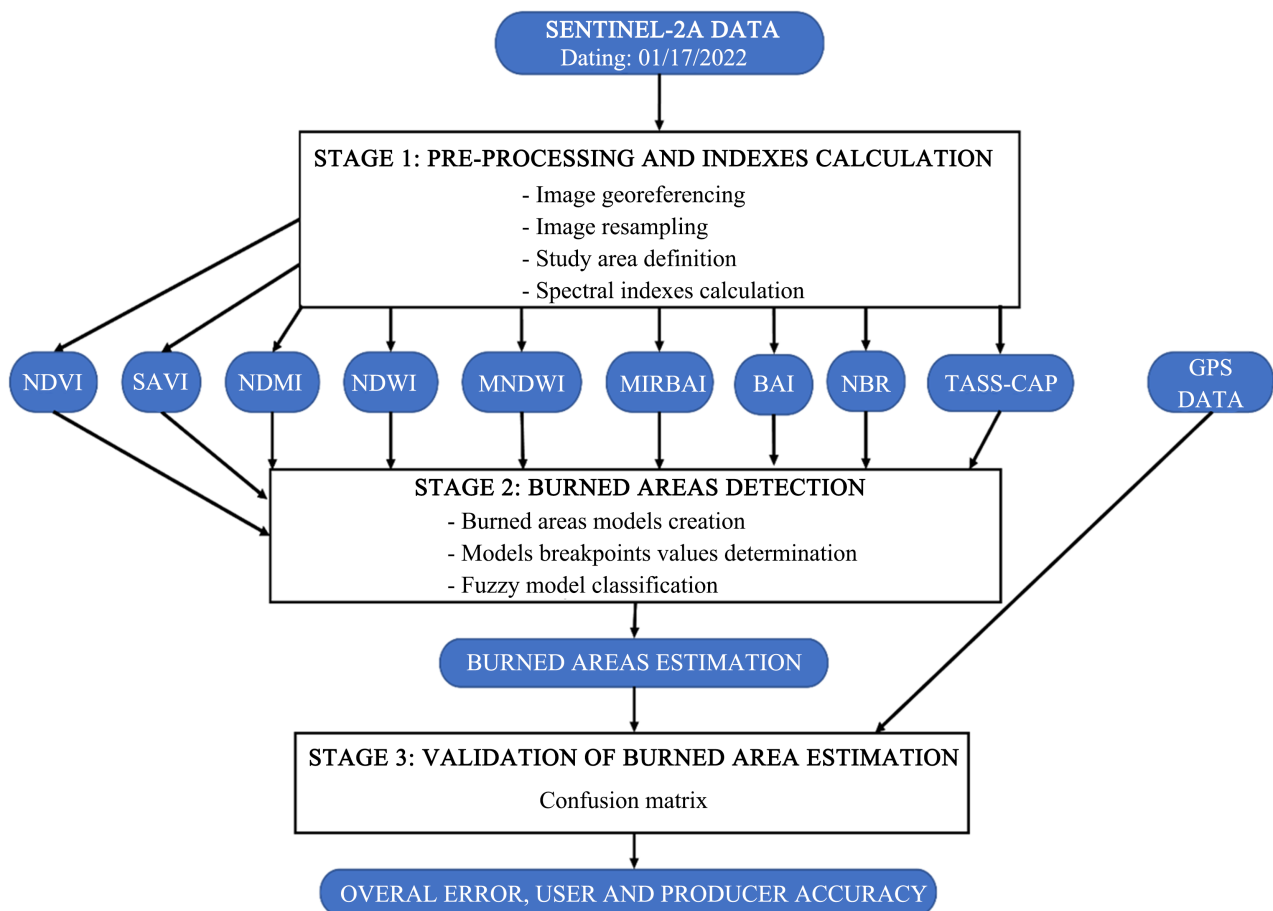


Figure 3. Summary of the methodology for various image processing steps.

For vegetation indices (NDVI, SAVI, TCG), three entities are observed, ranging from a red hue to a whitish hue. Whitish areas indicate high chlorophyll activity, corresponding to wooded savannah, open forests, and gallery forests. Red-toned areas indicate low chlorophyll activity, characterizing degraded savannah. Dark red or black-toned areas reveal an absence or very little vegetation cover, potentially representing water surfaces or mineral areas. For the interpretation of water or humidity indices (MNDWI, NDWI, NDMI, TCW), whitish areas would indicate water presence, while other hues would be attributed to vegetation and bare surfaces. For the bare soil index (TCB), whitish areas would represent bare surfaces, while other hues would represent vegetation and water surfaces. Regarding burn indices (MIRBI, BAI, NBR), whitish areas could represent areas with ash presence after a fire, while red or dark red areas indicate low or complete absence of ash.

4.2. Estimation and Validation of Burned Areas

Fuzzy classification was applied to various indices and sub-indices based on the degree of membership α to distinguish burned and unburned areas. The classification confusion matrix was calculated by comparing the results of the fuzzy

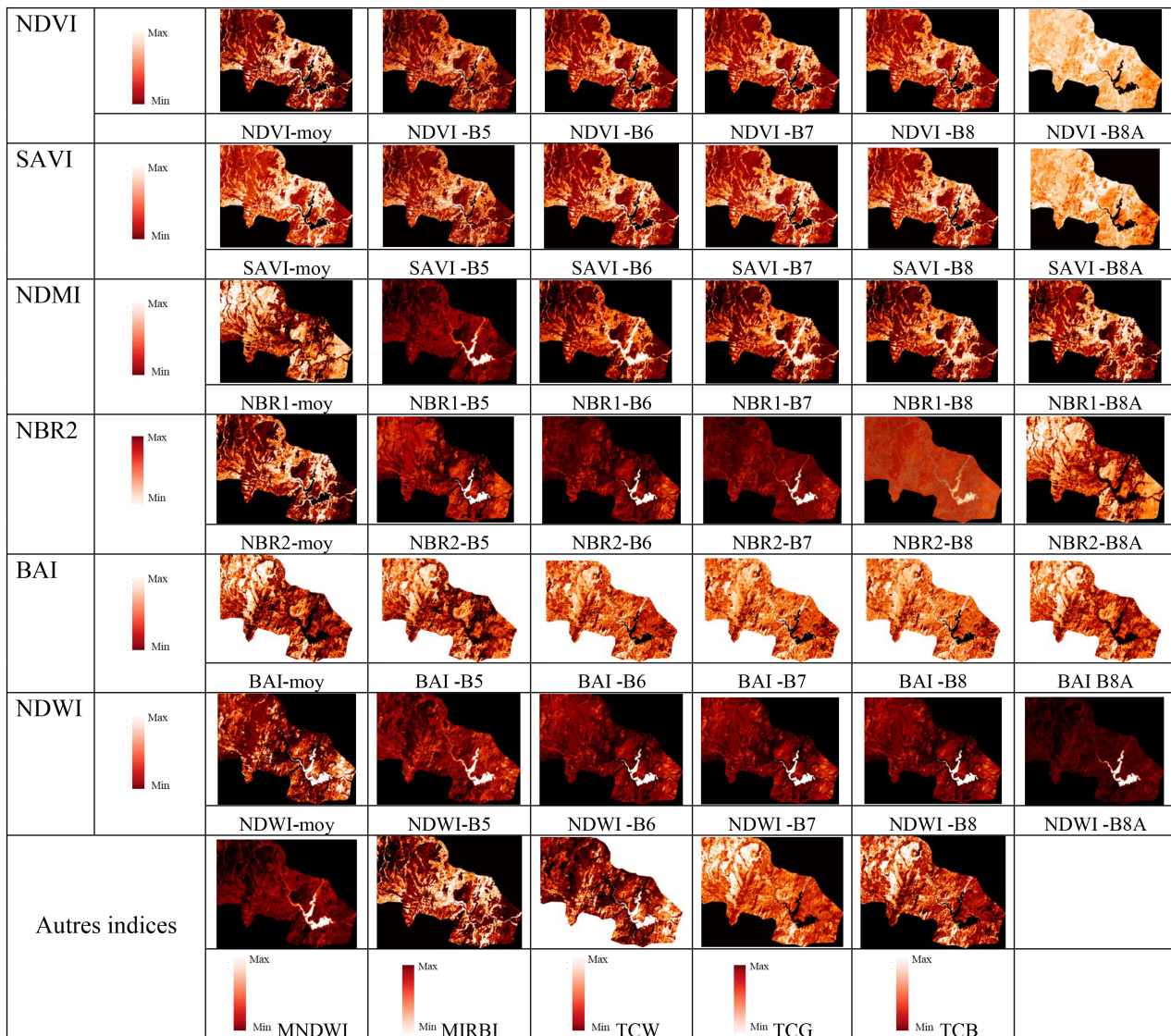


Figure 4. Spectral indices and sub-indices produced from the raw sentinel-2A Image.

classification with ground control data (ground truth). The achieved accuracies are presented in **Table 3**. The best overall accuracies obtained from the classification of indices and sub-indices are shown in **Table 7**.

Intra-index analysis reveals that as α approaches 1, the overall accuracy increases for all spectral indices, while it decreases as α approaches 0. These trends reflect a conservative behavior that reduces false alarms at the expense of a higher rate of missed burned areas. Inter-index analysis shows that classifying the mean indices yields satisfactory results in terms of overall classification accuracy compared to classifying each sub-index individually. The overall accuracies of the mean indices are nearly identical to those obtained from sub-indices derived from band 8. Therefore, using the mean indices is equivalent to directly using the sub-indices from band 8. However, the highest accuracy (97.20%) was achieved with the mean NDVI (NDVI-moy), followed by the mean SAVI

Table 7. Overall accuracies obtained from the classification of indices and sub-indices.

Spectral Indexes	Overall Accuracy (%)					
	$\alpha = 1$	$\alpha = 0.8$	$\alpha = 0.6$	$\alpha = 0.4$	$\alpha = 0.2$	$\alpha = 0$
NDVI-moy	97.2	96.3	95.4	94.1	93.2	92.5
NDVI-b8	95.5	94.8	93.7	92.2	91.6	90.5
SAVI-moy	94.1	93.2	92.5	91.5	90.6	89.3
SAVI-b8	93.4	92.1	91.4	90.2	89.1	88.8
NDMI-moy	90.2	89.3	88.3	88.3	88.3	88.3
NDMI-b8	89.9	88.8	87.1	87.1	87.1	87.1
NDWI-moy	80.3	79.1	77.3	77.1	76.7	75.3
NDWI-b8	80.1	79.2	78.1	76.8	76.1	75.0
NBR-moy	75.8	73.8	73.3	72.8	71.7	70.9
NBR-b8	75.3	73.1	72.3	71.6	70.6	69.5
BAI-moy	70.9	70.1	69.9	69.1	68.8	67.6
BAI-b8	69.5	68.9	68.5	67.5	66.8	66.4
MNDWI	78.4	77.2	77.3	77.2	76.4	75.3
TCW	79.2	79.1	78.3	77.1	76.8	75.2
TCG	81.3	80.2	80.1	79.8	78.3	77.6
TCB	62.9	61.8	61.3	60.9	60.6	59.8

(SAVI-moy) (95.50%) and the mean NDMI (NDMI-moy) (90.20%), while the lowest accuracy (62.90%) was obtained with the TCB index. These results differ from those of D. Stroppiana *et al.* [27], who found that NBR and CSI indices provide better discrimination of burned areas in the mediterranean region. Davide Fornacca *et al.* [14] also found that NBR is the index that best characterizes burned areas in a region in China. Wenliang Liu *et al.* [13] found that NDVI provides good classification results when combined with NBR. This situation can be explained by the fact that, in savannah regions like WAR, it is difficult to identify burned area using traditional fire indices like NBR, BAI, MIRBI, etc., because just after fires, the great part of ash disappears with the wind. In contrast, vegetation in of mediterranean and temperate regions the traces of fire are easily recognized by traditional fire indices. This confirms the idea that the choice of the index for characterizing burned areas differs depending on the physical and biological characteristics of the components of a given environment. The estimated burned areas resulting from the classification of the best spectral indices are recorded in **Figure 5**.

The burned areas detected by the mean NDVI, SAVI, and NDMI indices for a degree of membership $\alpha = 1$ are 2144.38 ha, 1932.14 ha, and 4947.13 ha, respectively.

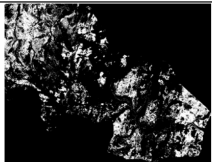
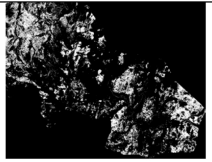

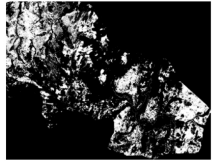
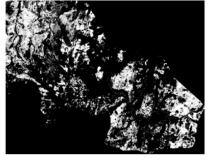

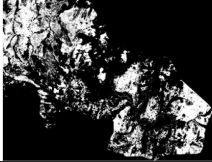
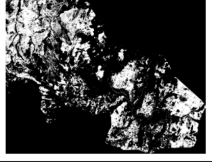

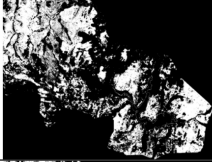
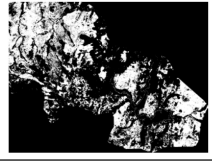

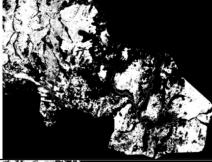
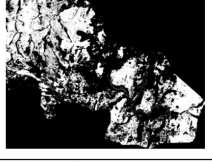

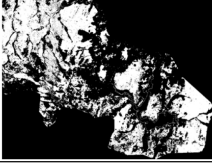


Degree of membership (α)	NDVI-moy	DAVI-moy	NDMI-moy
$\alpha = 1$			
$\alpha = 0.8$			
$\alpha = 0.6$			
$\alpha = 0.4$			
$\alpha = 0.2$			
$\alpha = 0$			

Figure 5. Burned areas for Mean NDVI, SAVI, and NDMI indices.

5. Conclusions

In this study, we set out to enhance our understanding of burned areas by harnessing the potential of spectral indices and employing a fuzzy classification approach. This approach allows for a more nuanced evaluation of the data, offering a range of degrees of membership (α) that enables a fine-tuned analysis of the results.

The outcomes of our research revealed a consistent trend: as the degree of membership α decreased from 1 to 0, the accuracy of all the spectral indices gradually declined. However, two indices, NBR and BAI, exhibited an interesting exception to this pattern. These indices maintained their accuracy across the range of α values.

Furthermore, we observed that the mean spectral indices, specifically NDVI, SAVI, NDMI, and NDWI, consistently outperformed their individual counterparts in terms of classification results. These mean spectral indices exhibited remarkable sensitivities of 86%, 85%, 82%, and 81%, respectively, demonstrating

their robustness in identifying burned areas. Moreover, they achieved high accuracies of 95%, 94%, 92%, and 90%, indicating the reliability of these composite indices in accurately characterizing the extent of fire-affected areas.

It's noteworthy that these results, while highlighting the efficiency of these mean spectral indices, did not significantly differ from the performance of individual indices, with sensitivities ranging from 79% to 84%, and accuracies ranging from 87% to 93%. This suggests that, whether through the combination of indices or the use of individual ones, our approach can effectively contribute to the precise discrimination of bushfires in Côte d'Ivoire.

The date of image acquisition (January) and field data collection could be some limitations for the study, because, at that date, all the bushfires in the WAR had not been completed. As a result, burned areas may be underestimated. The results of the study could be supplemented by others detections of burned areas using some images of February and early March.

In conclusion, the findings of this study offer valuable insights for fire management and monitoring in the region. By applying fuzzy classification and carefully selecting or averaging spectral indices, we have improved the accuracy and reliability of burned area identification. These results can significantly aid the efforts to understand, predict, and mitigate the impact of bushfires in Côte d'Ivoire and other regions facing similar challenges.

Conflicts of Interest

The authors declare no conflicts of interest regarding the publication of this article.

References

- [1] Doerr, S.H., Santín, C., Trans, R. and Soc, B. (2016) Global Trends in Wildfire and Its Impacts: Perceptions versus Realities in a Changing World. *Philosophical Transactions of the Royal Society B: Biological Sciences*, **371**, 1-10. <https://doi.org/10.1098/rstb.2015.0345>
- [2] Giglio, L., Loboda, T., Roy, D.P., Quayle, B. and Justice, C.O. (2009) An Active-Fire Based Burned Area Mapping Algorithm for the MODIS Sensor. *Remote Sensing of Environment*, **113**, 408-420. <https://doi.org/10.1016/j.rse.2008.10.006>
- [3] Kouassi, J.-L., Wandan, N. and Mbow, C. (2022) Exploring Wildfire Occurrence: Local Farmers' Perceptions and Adaptation Strategies in Central Côte d'Ivoire, West Africa. *Journal of Sustainable Forestry*, **41**, 173-192. <https://doi.org/10.1080/10549811.2020.1845744>
- [4] Kouassi, J.-L., Wandan, N. and Mbow, C. (2022) Exploring Spatio-Temporal Trends and Environmental Drivers of Wildfire Occurrence and Impacts in Côte d'Ivoire, West Africa. *African Journal of Ecology*, **60**, 1218-1236. <https://doi.org/10.1111/aje.13066>
- [5] Mbow, C., Goïta, K. and Bénié, G.B. (2004) Spectral Indices and Fire Behavior Simulation for Fire Risk Assessment in Savanna Ecosystems. *Remote Sensing of Environment*, **91**, 1-13. <https://doi.org/10.1016/j.rse.2003.10.019>
- [6] Aubréville, A. (1953) Les expériences de reconstitution de la savane boisée en Cote

- d'Ivoire. Bois et Forêts des Tropiques. 32.
- [7] Louppe, D., Ouattara, N. and Coulibaly, A.B. (1995) Effets des feux de brousse sur la végétation. Bois et Forêts des tropiques. 245.
- [8] Agoualé, Y.J. (2017) Influence des feux de brousse sur l'évolution des paysages forestiers dans la réserve de faune d'Abokouamékro. *International Journal of Innovation and Scientific Research*, **31**, 1-6.
- [9] Barry, M.B., Badiane, D., Diakhaté, M., Sall, S.M., Senghor, H. and Millimono, T.N. (2018) Variability and Predictability of Bush Fire in Guinea on Inter-Annual and Multi-Year Timescales Based on NDVI-MODIS Datasets Analysis. *African Journal of Environmental Science and Technology*, **12**, 514-522. <https://doi.org/10.5897/AJEST2018.2562>
- [10] Afelu, B., Fontodji, K.J., Kokou, K. and Kokou, J.F. (2016) Impact des feux sur la biomasse dans les savanes guinéo-soudaniennes du Togo [Vertigo]. *La Revolution électronique en Science l'environnement*, **16**, 1-27. <https://doi.org/10.4000/vertigo.17106>
- [11] Joachim, E. and Collins, K. (2007) Apport de trois méthodes de détection des surfaces brûlées par imagerie Landsat ETM+: Application au contact forêt. savane du Cameroun.
- [12] Doe, J., Smith, J. and Johnson, M. (2020) Burned Area Detection Using Sentinel-2A Satellite Imagery and Spectral Indices. *Remote Sensing*, **789**, 96-106.
- [13] Liu, W., Wang, L., Zhou, Y., Wang, S., Zhu, J. and Wang, F. (2015) A Comparison of Forest Fire Burned Area Indices Based on HJ Satellite Data. *Natural Hazards*, **81**, 971-980. <https://doi.org/10.1007/s11069-015-2115-x>
- [14] Fornacca, D., Ren, G. and Xiao, W. (2018) Performance of Three MODIS Fire Products (MCD45A1, MCD64A1, MCD14ML), and ESA Fire_CCI in a Mountainous Area of Northwest Yunnan, China, Characterized by Frequent Small fires. *Remote Sensing*, **9**, 1131. <https://doi.org/10.3390/rs9111131>
- [15] Martinez, A. and Rodriguez, C. (2019) Improved Burned Area Mapping in Mediterranean Ecosystems Using Sentinel-2A Data. *International Journal of Remote Sensing*, **12**, 3854-3873.
- [16] Khan, A. and Miller, S. (2018) Deep Learning-Based Burned Area Detection from Sentinel-2A Imagery. *IEEE Transactions on Geoscience and Remote Sensing*, **16**, 2188-2197.
- [17] Perez, L. and Johnson, R. (2017) Integration of Multispectral and Thermal Infrared Data from Sentinel-2A for Improved Burned Area Detection. *Remote Sensing of Environment*, **36**, 1-14.
- [18] Davis, E. and Walker, S. (2019) Change Detection of Burned Areas Using Sentinel-2A Time Series Data. *ISPRS Journal of Photogrammetry and Remote Sensing*, **4**, 166-177.
- [19] Davis, M. and Wilson, E. (2020) A Machine Learning Approach for Rapid Burned Area Assessment with Sentinel-2A Data in Disaster Response. *Natural Hazards and Earth System Sciences*, **16**, 419-431.
- [20] Gonzalez, M., Rodriguez, C., *et al.* (2018) Evaluation of Sentinel-2A Data for Burned Area Mapping in Arid Regions. *Remote Sensing*, **10**, 1570.
- [21] Walker, A. and Lopez, M. (2017) Spatiotemporal Analysis of Burned Area Using Sentinel-2A Data: Case Studies in Different Ecosystems. *International Journal of Applied Earth Observation and Geoinformation*, **22**, 70-82.
- [22] Smith, B. and Miller, E. (2019) An Ensemble Approach for Burned Area Mapping

- from Sentinel-2A Data. *Remote Sensing of Environment*, **50**, 149-162.
- [23] Brown, D. and Perez, L. (2018) Mapping Burned Area Severity with Sentinel-2A: A Geospatial Analysis Approach. *Journal of Applied Remote Sensing*, **88**, 14-26.
- [24] Garcia, S. and Brown, D. (2016) Comparative Analysis of Pre- and Post-Fire Sentinel-2A Imagery for Burned Area Mapping. *IEEE Geoscience and Remote Sensing Letters*, **25**, 1715-1719.
- [25] Smith, J. and Smith, A. (2017) Assessing the Accuracy of Burned Area Mapping in Urban Areas Using Sentinel-2A Data. *Urban Remote Sensing*, **98**, 100-110.
- [26] Avenard, J.M. (1971) *Le milieu naturel de la Côte d'Ivoire*: IRD Editions.
- [27] Stroppiana, D., Pinnock, S., Pereira, J.M.C. and Grégoire, J.M. (2002) Radiometric Analysis of Spot-Vegetation Images for Burnt Area Detection in Northern Australia. *Remote Sensing of Environment*, **82**, 21-37.
[https://doi.org/10.1016/S0034-4257\(02\)00021-4](https://doi.org/10.1016/S0034-4257(02)00021-4)